


Article

Effect of Calcination Temperature on Photocatalytic Activity of Synthesized TiO₂ Nanoparticles via Wet Ball Milling Sol-Gel Method

Siripond Phomma ¹, Tuksadon Wutikhun ², Panita Kasamechonchung ², Tippabust Eksangsri ¹ and Chaweewan Sapcharoenkun ^{2,*}

¹ Department of Chemical Engineering, Faculty of Engineering, Thammasat University, Pathumthani 12120, Thailand; siripond_may@hotmail.com (S.P.); etippabu@engr.tu.ac.th (T.E.)

² National Nanotechnology Center (NANOTEC), National Science and Technology Development Agency (NSTDA), Thailand Science Park, Phahonyothin Rd., Khlong Nueng, Khlong Luang, Pathumthani 12120, Thailand; tuksadon@nanotec.or.th (T.W.); panita@nanotec.or.th (P.K.)

* Correspondence: chaweewan@nanotec.or.th; Tel.: +66-02-117-6586

Received: 8 January 2020; Accepted: 29 January 2020; Published: 3 February 2020



Abstract: In this work, TiO₂ nanoparticles were successfully synthesized with narrow size distribution via a wet ball milling sol-gel method. The effect of calcination temperature on photocatalytic activity was observed from particle size, crystallite size, and phase transition of TiO₂ nanoparticles. Increasing calcination temperature increased particle size, crystallite size, and the crystallinity of synthesized TiO₂. Phase transition depended on variation in calcination temperatures. A two-phase mixture of anatase and brookite was obtained with lower calcination temperature whereas a three-phase mixture appeared when calcination temperature was 500–600 °C. With higher temperature, the rutile phase kept increasing until it was the only phase observed at 800 °C. Anatase strongly affected the photocatalytic activity from 300 °C to 600 °C while the particle size of TiO₂ was found to have a dominant effect on the photocatalytic activity between 600 °C and 700 °C. A mixture of three phases of TiO₂-600 exhibited the highest methylene blue degradation with the rate constant of $9.46 \times 10^{-2} \text{ h}^{-1}$ under ultraviolet (UV) irradiation.

Keywords: TiO₂ nanoparticle; calcination temperature; phase transition; particle size; photocatalytic activity

1. Introduction

Titanium dioxide (TiO₂) photocatalyst has been extensively studied and widely applied in water and air treatment [1], paint [2], protective coatings [3], and cosmetics [4]. There are many advantages of TiO₂ such as chemical stability, self-cleaning, biocompatibility, and strong antibacterial qualities. TiO₂ with high photocatalytic and strong antibacterial activities has attracted much attention in decades [5]. TiO₂ photocatalyst has three polymorph structures, namely anatase, rutile, and brookite. High photocatalytic activity of TiO₂ under ultraviolet (UV) light is strongly depended on phase composition, crystallinity, crystallite size, and surface area [6,7]. The relationship between TiO₂ phase and its photocatalytic activity has been an interest for many researchers. Although pure anatase phase of TiO₂ has been preferred, there is a limitation of fast recombination of photogenerated electrons (e⁻) and holes (h⁺). Some works have shown that the mixture of anatase-rutile [8–11], anatase-brookite [12,13] and brookite-rutile [14,15] phases of TiO₂ powder in a certain ratio provided higher photocatalytic activity than the pure phase. Kangle et al. [11] found that the mixture of anatase and rutile phases with a ratio of 57:43 provides the highest hydroxyl radical (OH) formation and photocatalytic activity under UV irradiation. Kandiel et al. [12] studied methanol photo-oxidation of TiO₂ powder and found

that the mixture of anatase-brookite phases of TiO_2 showed higher photocatalytic activity than pure anatase phase. Cao et al. [14] determined that the highest photodegradation of phenol was achieved by using TiO_2 composed of 72% of brookite and 28% of rutile. Although binary phases of TiO_2 provided higher photocatalytic activity than pure phase, there have been reports that ternary phases present higher photocatalytic activity than single [16] and binary phases [17]. Paola et al. [16] investigated that the mixture of three phases including 65% anatase, 28% brookite, and 7% rutile phase showed higher photocatalytic activity degradation of 4-nitrophenol than pure rutile phase. Liao et al. [17] found that the mixture of 30% anatase, 28% brookite, and 42% rutile showed higher photocatalytic activity over 90% degradation of methyl orange solution in 20 min than the mixture of anatase and rutile phase. The effect of synergetic phase junction and different band alignments of each phase provides e^- and h^+ transfer at the interface of TiO_2 . This can enhance e^- - h^+ separation and reduce e^- - h^+ recombination leading to an enhanced photocatalytic activity under UV light. However, a relationship between synthesis condition and mixture ratio of multiple phases of TiO_2 has still been a challenge for high photocatalytic activity.

There are many synthesis methods such as hydrothermal [18], microwave [19], supercritical antisolvent [20], and sol-gel [21] methods for preparation of TiO_2 nanoparticles. Hydrothermal, microwave, and supercritical antisolvents provided high purity and high surface equipment for TiO_2 synthesis, whereas the sol-gel method can be undertaken at atmospheric pressure and room temperature. The sol-gel method is one of the promising methods for large-scale production [22]. However, this method suffers from controlling the shape and size distribution of TiO_2 nanoparticles. Generally, the smaller the particle size of TiO_2 leads to the larger surface area and higher photocatalytic activity under UV light irradiation. A grinding process is required for the high surface area of TiO_2 powder. Dry ball milling has been used widely to reduce the size of nanoparticles. However, wet ball milling provides smaller particle size and narrower size distribution [23]. Jung et al. [24] found that the size of TiO_2 particles was decreased and showed a uniform size distribution by using a wet ball milling process. Furthermore, phase, crystallite size, and crystallinity of TiO_2 play a critical role for high photocatalytic activity which they can be governed by calcination temperature in the sol-gel method. Behnajady et al. [25] reported the effect of calcination temperature on a phase transition of TiO_2 from anatase to rutile at calcination temperatures from 350 °C to 750 °C. Mutuma et al. [26] investigated that the mixture of anatase and brookite phases was found at a calcination temperature of 200 °C. The mixture of three phases was found at 600 °C and completely transfer to rutile phase at 800 °C. Moreover, crystallite size and crystallinity of TiO_2 were increased when calcination temperature increased [27,28]. However, explanation to understand the crystallite size and phase transformation of TiO_2 which affect photocatalytic activity is still limited.

In this work, TiO_2 particles were synthesized by the wet ball milling sol-gel (WBMS) method [29]. The effect of calcination temperature on photocatalytic activity was investigated. The crystallinity, particle size, and phase transition of synthesized TiO_2 have been all observed in order to provide more understanding of phase mixture for photocatalytic activity.

2. Materials and Methods

2.1. Preparation of TiO_2 and Characterization of Synthesized TiO_2 Material

The effect of calcination temperature on TiO_2 synthesis with WBMS: TiO_2 was synthesized which was modified from the previous report of Bahadur et al. [30]. In this work, methanol (Thermo Fisher Scientific, Waltham, MA, USA) was used as a solvent for TiO_2 synthesis from previous study [29] because the smallest particle size, the narrowest size distribution and the highest photocatalytic degradation of methylene blue could be achieved when compared to ethanol and isopropanol. Commercial P25 TiO_2 (89% anatase and 11% rutile) (Kanto Chemical Co., Inc., Tokyo, Japan) was used as a TiO_2 reference and purchased from ACROS. A diagram of the TiO_2 synthesis via the WBMS method is shown in Figure 1. The substitution reaction of 97%wt.-titanium tetraisopropoxide (TTIP) (Sigma-Aldrich Pte

Ltd., Singapore) with 99.99%wt.-methanol (MeOH) (Sigma-Aldrich Pte Ltd., Singapore) was carried out with a molar ratio of TTIP:MeOH of 1:15. Then the hydrolysis reaction of titanium alkoxide was carried out by adding deionized water (DI) with a molar ratio of TTIP:DI water of 1:4. The solution pH was adjusted to 1.5 by adding 65%wt. concentrated HNO₃ (Carlo Erba reagents S.A.S, Val-de-Reuil, France). The white colloid of TiO₂ sol was observed. The TiO₂ gel mixture was washed with DI water and centrifuged at 10,000 rpm for 15 min. The white jelly-like gel was dried in an oven (Memmert GmbH & Co.KG, Schwabach, Germany) at 110 °C for 24 h to remove organic solvents. The yellow-light xerogel was dry ground with 10 mm-ball milling at 300 rpm for 20 min and consequently wet ground by 2 mm-ball milling at 500 rpm for 3 h in isopropanol. The TiO₂ solution was then dried in the oven at 110 °C for 24 h. The synthesized particles were calcined at different temperatures of 300, 400, 500, 600, 650, 700, and 800 °C for 4 h with a heating rate of 5 °C/min and labeled as TiO₂-300, TiO₂-400, TiO₂-500, TiO₂-600, TiO₂-650, TiO₂-700, and TiO₂-800, respectively.

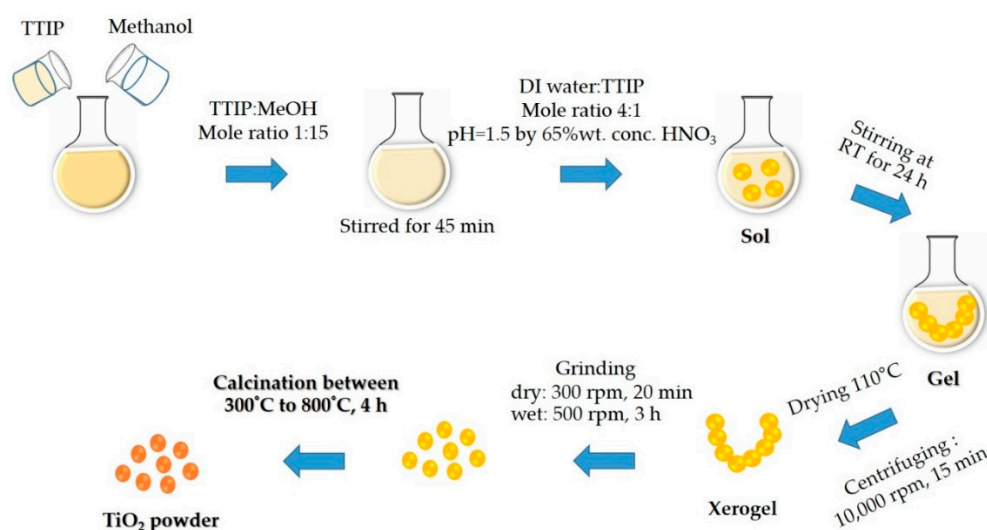


Figure 1. Synthesis of TiO₂ nanoparticles via wet ball milling sol-gel (WBMS) method.

2.2. Characterizations of TiO₂

The morphology, particle size, and phase of TiO₂ powder were studied using transmission electron microscope (TEM) (JEM-2100, JEOL Ltd., Tokyo, Japan, software of 2013) operated at 200 kV. X-ray diffraction (XRD) (D8 Advance, Bruker, Germany) patterns were obtained with a Bruker D8 ADVANCE equipped with Cu source (Cu K α = 0.154 nm, 40 kV, 40 mA). The scattered radiation was detected in the angular range of 10–80° (2 θ) with a scan rate of 0.02°. A commercial Total Pattern Analysis Solution software (TOPAS version 4.2, Bruker, Germany, 2011) was employed to determine the crystallite size and phase content of TiO₂ powder. The absorption edge and energy band gap of TiO₂ were investigated by diffuse reflectance spectroscopy (DRS) (Cary Series, Agilent Technologies, Santa Clara, CA, USA) with the wavelength range of 200–800 nm (Agilent carry 5000). The energy band gap of synthesized TiO₂ with different calcination temperatures was calculated by using Tauc plot from the equation as follows:

$$(\alpha h\nu)^{\frac{1}{n}} = A(h\nu - E_g) \quad (1)$$

where α is the extinction coefficient, h is the Planck's constant (J·S), ν is the light frequency (s⁻¹), A is the absorption constant, E_g is the energy band gap (eV) and n is the value of the specific transition, $n = 2$ for indirect band gap, and $n = \frac{1}{2}$ for direct band gap [31].

2.3. Photocatalytic Activity Reaction

The degradation of methylene blue (MB) (Ajax Finechem) under UV irradiation was used as a model system to evaluate the photocatalytic performance of TiO₂ powder. The photocatalytic reaction

was carried out in the in-house photocatalytic chamber. The initial concentration of MB (C_0) was prepared at 5 ppm. 10 mg of TiO_2 was mixed with 40 mL of MB solution and then stirred in the photocatalytic chamber. The mixture was kept in the dark for 1 h to ensure the saturation of MB on the surface of the catalysts. The MB solution was irradiated by 0.25 mWcm^{-2} with UV light ($\lambda = 351 \text{ nm}$). The sample was collected every hour for 28 h. The concentration of MB in suspension was analyzed using an ultraviolet–visible (UV–Vis) spectrophotometer with the wavelength of maximum absorbance at 664 nm. The kinetic constants of reaction rate were determined according to the pseudo-first-order kinetic model as follows:

$$\ln\left(\frac{C}{C_0}\right) = -kt \quad (2)$$

where t is the irradiation time (h), k is kinetic constant (h^{-1}), C_0 is the initial concentration (mg/L), and C is the concentration of the MB (mg/L) at certain irradiation time.

3. Results and Discussion

The morphology, particle size, and phase of synthesized TiO_2 with different calcination temperatures were investigated by transmission electron microscopy (TEM) as shown in Figure 2. It was observed that TiO_2 -300, TiO_2 -600, and TiO_2 -700 showed the mixture of spherical, cubic, and hexagonal shapes while TiO_2 -800 provided an almost hexagonal shape with the agglomeration and aggregation of particles. The particle size of TiO_2 -300, TiO_2 -600, TiO_2 -700, and TiO_2 -800 particles were 8.6 ± 1.7 , 18.7 ± 3.7 , 27.6 ± 8.2 , and $81.6 \pm 21.6 \text{ nm}$, respectively. It was observed that increasing calcination temperature leads to increasing particle size and crystallite size of TiO_2 particles. At low calcination temperature of $300 \text{ }^\circ\text{C}$, the mixture of anatase (101) and brookite (111) phases with d-spacing of 3.520 and 3.465 nm was observed for TiO_2 -300 (Figure 2a). When increasing calcination temperature to $600 \text{ }^\circ\text{C}$ (Figure 2b), there were three phases composed of anatase (101), brookite (111), and rutile (110) with d-spacing of 3.520, 3.465, and 3.247 nm, respectively. TiO_2 -700 (see Figure 2c) showed the mixture of anatase (101) and rutile (200) phases with d-spacing of 3.520 nm and 2.297 nm, respectively. TiO_2 -800 showed only rutile phase (110) with d-spacing of 3.247 nm as shown in Figure 2d. Moreover, inset images in Figure 2 show selected area electron diffraction (SAED) images of TiO_2 particles. The results demonstrated that there was a mixture of anatase (211) and brookite (221) phases observed for TiO_2 -300. When calcination temperature was increased from $300 \text{ }^\circ\text{C}$ to $600 \text{ }^\circ\text{C}$, there were three phases composed of anatase (101), rutile (111), and brookite (113) phases. SAED patterns showed anatase (220) and rutile (210) phases for TiO_2 -700 and showed only the rutile (210) phase for TiO_2 -800. Figure 2b–d showed that increasing of calcination temperature from $600 \text{ }^\circ\text{C}$ to $800 \text{ }^\circ\text{C}$ increased the aggregation of crystallites leading to larger crystallite size and lower surface area since the anatase and brookite phases were completely transformed to the rutile phase. This indicates that crystallite size of TiO_2 powder was increased at high temperature due to larger crystallite size of the rutile phase. It was reported that the most stable crystallite size of anatase and brookite phases is less than 11 nm and 11–35 nm, respectively, while the most stable crystallite size of the rutile phase is larger than 35 nm [32]. In addition, with increasing calcination temperature the crystallinity was increased. This can be attributed to the thermally promoted crystallite growth. Therefore, TEM and SAED images confirmed phase synthesis of TiO_2 powder strongly depend on calcination temperature. At low calcination temperature, anatase and brookite phases were presented. Phase transition of TiO_2 to rutile phase was significant when the calcination temperature was higher.

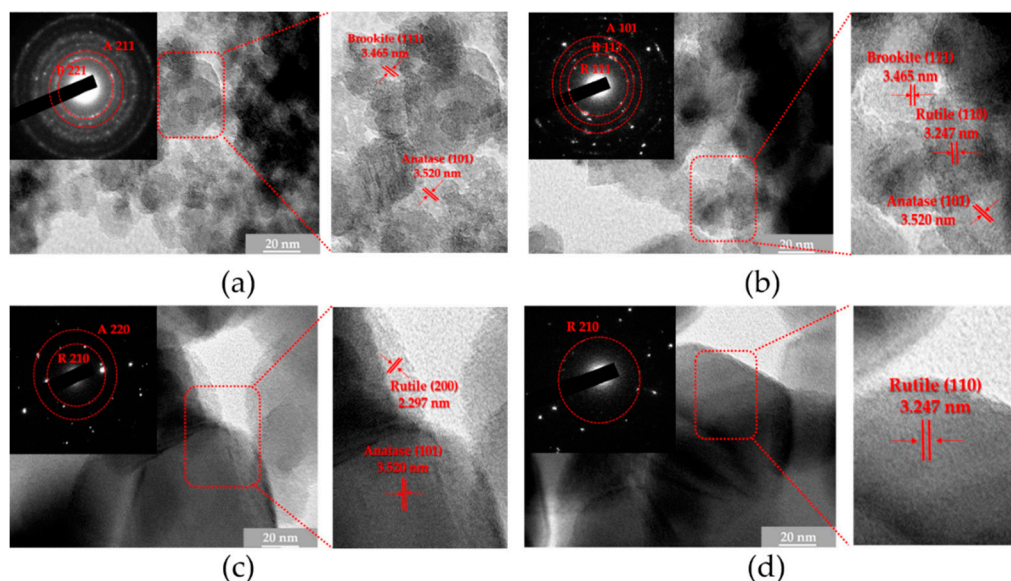


Figure 2. Transmission electron microscope (TEM) images and selected area electron diffraction (SAED) (inset) images of each TiO_2 particles calcined at (a) 300 °C, (b) 600 °C, (c) 700 °C, and (d) 800 °C.

XRD patterns of synthesized TiO_2 particles before and after calcination at different temperatures from 300 °C to 800 °C are shown in Figure 3. Anatase phase is the tetragonal structure and consists of the characteristic peaks at $2\theta = 25.3^\circ, 36.9^\circ, 37.8^\circ, 55.1^\circ,$ and 70.3° corresponding to (101), (103), (004), (211), and (220) planes, respectively referenced from the Joint Committee on Powder Diffraction Standard (JCPDS card no. 21-1272). The rutile phase is also a tetragonal structure and presents diffraction peaks at $2\theta = 27.4^\circ, 36.1^\circ, 39.2^\circ, 41.2^\circ, 44.0^\circ, 54.3^\circ, 56.6^\circ, 62.7^\circ, 64.0^\circ, 69.0^\circ,$ and 69.8° corresponding to (110), (101), (200), (111), (210), (211), (220), (002), (310), (301), and (112) planes, respectively (JCPDS card no. 21-1276). Orthorhombic as shown in the brookite phase presents diffraction peaks at $2\theta = 25.3^\circ, 25.7^\circ, 36.2^\circ, 42.3^\circ, 55.2^\circ$ and 57.2° corresponding to (120), (111), (012), (221), (241), and (113) planes, respectively (JCPDS card no. 29-1360). The broader peaks of XRD patterns were observed before calcination and after calcination from 300 °C to 500 °C. This could be attributed to high amorphous structure of TiO_2 . Increasing calcination temperature above 600 °C, it was found that the crystallinity of TiO_2 increased due to the sharper and narrower peaks of XRD patterns. The crystallinity increased with increasing calcination temperature since higher ordering of the structure of TiO_2 particles leads to the sharper and narrower X-ray peaks. Besides, the crystallite size of all phases increased with increasing calcination temperature which indicates that the crystallization of TiO_2 was improved as shown in Table 1. These results from XRD also confirm and agree well with the TEM results as previously mentioned. Therefore, calcination temperature promoted phase transition, crystallite size, and crystallinity of TiO_2 powder.

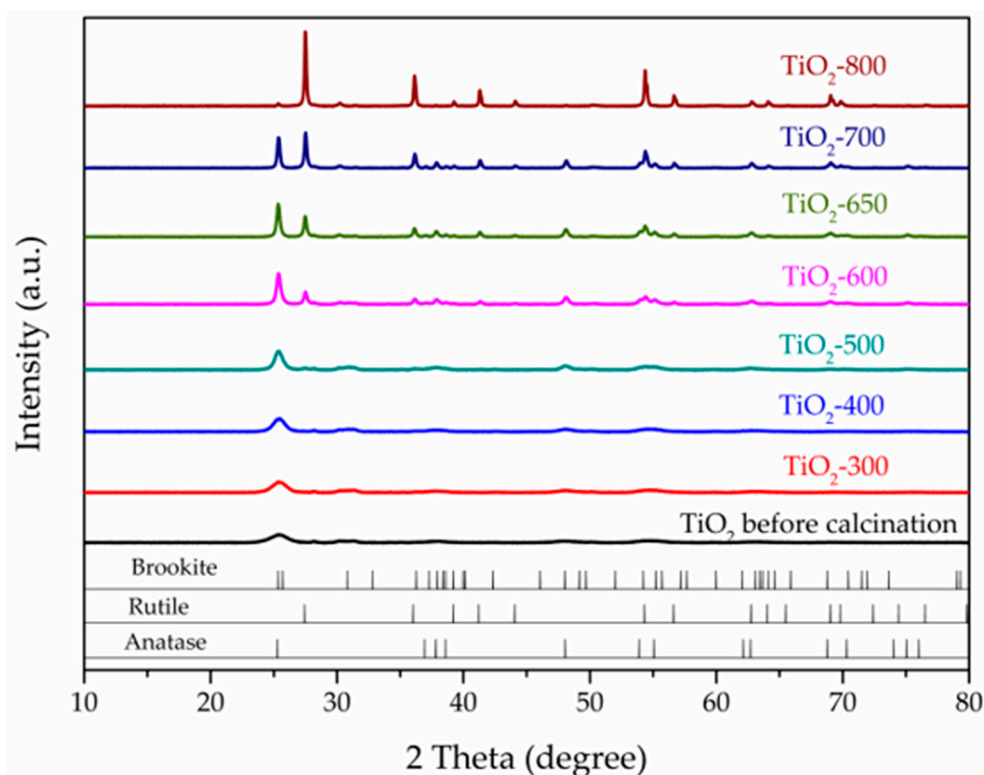


Figure 3. X-ray diffraction (XRD) patterns of TiO₂ particles before and after calcination at different temperatures ranging from 300 °C to 800 °C.

Table 1. Crystallite size and energy band gap of synthesized TiO₂ particles before and after calcination and commercial P25 TiO₂.

Sample	Crystallite Size (nm)			Energy Band Gap (eV)
	Anatase	Rutile	Brookite	
TiO ₂ before calcination	6	-	3	-
TiO ₂ -300	7	-	4	3.10 ± 0.03
TiO ₂ -400	8	-	5	3.29 ± 0.04
TiO ₂ -500	12	4	5	3.28 ± 0.03
TiO ₂ -600	20	19	6	3.16 ± 0.02
TiO ₂ -650	23	25	-	3.08 ± 0.02
TiO ₂ -700	30	32	-	3.07 ± 0.02
TiO ₂ -800	-	52	-	3.05 ± 0.01
P25	17	28	-	-

The weight percentage of anatase, rutile, and brookite phases of synthesized TiO₂ by different calcination temperatures was estimated by TOPAS. The relationship between calcination temperature and percentage of phase content is shown in Figure 4a. When calcination temperature was increased from 300 °C to 600 °C, the anatase phase increased from 29% to 42%wt. whereas the brookite phase decreased from 71% to 28%wt. It is interesting to note that the brookite phase was observed at calcination temperature below 600 °C. It was reported that the brookite phase can be observed as a by-product in the sol-gel method in an acidic condition at low temperature [27]. These results corresponded well with other studies as shown in Table 2. There was a mixture of anatase and brookite phases when calcination temperature was increased from 300 °C to 400 °C. This result was correlated with the study of Mutuma et al. [26]. Considering calcination temperature between 600 °C and 700 °C, it was observed that the anatase phase decreased from 42% to 38%wt. whereas the rutile phase increased from 30% to 62%wt. The rutile phase was observed above 500 °C. This result was in good

agreement with the reports of Mutuma et al. [26], Bamme et al. [33] and Saalinraj et al. [34]. A mixture of the anatase and the rutile phases was found between 650 °C and 700 °C which was consistent with the study of Banjuraizah et al. [35]. The anatase and brookite phases were completely converted to the rutile phase at 800 °C because the rutile phase provided thermal stability at high temperature [34].

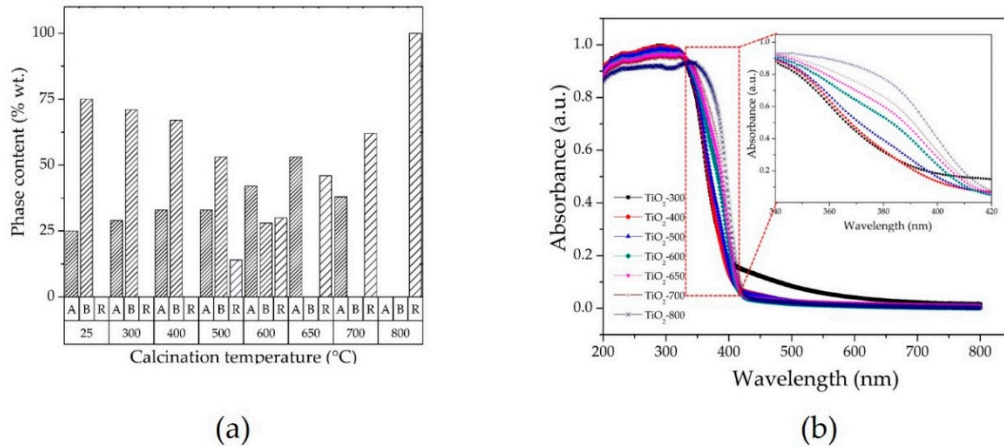


Figure 4. (a) Relationship between calcination temperature before and after calcination temperatures from 300 °C to 800 °C and percentage of phase content of synthesized TiO₂, (b) diffuse reflectance spectroscopy (DRS) spectra of TiO₂ with different calcination temperatures.

Table 2. Phase transition of TiO₂ synthesized via sol-gel method and calcined with different calcination temperatures.

Calcination Temperature	Comment	Reference
25–800 °C	Calcination temperature below 600 °C found the mixture of anatase and brookite phases. The rutile phase was found above 600 °C and only the rutile phase was found at 800 °C.	[26]
300–600 °C	Pure anatase phase was found between 300 °C and 400 °C. Rutile was found above 500 °C.	[33]
200–800 °C	Pure anatase was found between 200 °C and 400 °C. The rutile phase was found above 500 °C.	[34]
400–700 °C	Calcination temperature below 700 °C found only pure anatase and calcination temperature of 700 °C found the mixture of anatase and rutile phases.	[35]

Absorption edge of TiO₂ with different calcination temperatures was investigated by DRS as shown in Figure 4b. It was observed that absorption edge of TiO₂ between 320 nm and 440 nm showed red shift when calcination temperature was increased. The higher wavelength of absorption edge provides the lower energy band gap. Energy band gap of TiO₂ with direct band gap structure was determined using Tauc analysis as shown in Table 1. Bulk TiO₂ is an indirect band gap and direct transitions are forbidden by selection rules. However, due to the finite size of the TiO₂ nanoparticles, the origin of the transition does not necessarily reflect that occurring in the bulk. Therefore, direct or indirect transitions in TiO₂ nanoparticles can be presented [36,37]. It was observed that the mixture of three phases provided the energy band gap between 3.16 eV and 3.28 eV. While the mixture of anatase and rutile phases (3.07–3.08 eV) showed a lower energy band gap than the mixture of anatase and brookite phases (3.10–3.29 eV). This result agreed well with many studies in which rutile has been reported to have a band gap of about 3.0 eV and brookite has been reported to have a band gap between 3.0 eV and 3.6 eV. Anatase has been reported to have a band gap about 3.2 eV. The lowest energy band gap of TiO₂-800 composed of only the rutile phase is 3.05 eV and well correlated with the report of Da Silva et al. [20] who also found the energy band gap of the rutile phase was 3.05 eV.

The methylene blue adsorption capability of synthesized TiO₂ and P25 is shown in Figure 5a. Before UV light illumination, the solutions were kept in dark for 1 h under stirring to saturate the adsorption of MB. It was observed that the concentration of MB solutions of TiO₂-600, TiO₂-650, TiO₂-700, TiO₂-800, and P25 was reduced about 10% of initial MB solutions while TiO₂-300, TiO₂-400 and TiO₂-500 showed negligible adsorption capability of MB under dark condition. Figure 5b presents the study of photocatalytic activity of synthesized TiO₂ nanoparticles with different calcination temperatures from 300 °C to 800 °C and a comparison with commercial P25 TiO₂ nanoparticles as a reference. Table 3 shows the kinetic constant of MB degradation of synthesized TiO₂. The effect of calcination temperature on phase transition of synthesized TiO₂ powders provided the different kinetic constants as shown in Figure 6a. It was observed that P25 with 89:11 of anatase to rutile showed the highest photocatalytic activity with the kinetic constant of $11.41 \times 10^{-2} \text{ h}^{-1}$. However, among synthesized TiO₂, TiO₂-600 provided the highest photocatalytic activity with the kinetic constant of $9.46 \times 10^{-2} \text{ h}^{-1}$. Increasing calcination temperature from 300 °C to 400 °C, the kinetic constant increased from 2.54×10^{-2} to $3.87 \times 10^{-2} \text{ h}^{-1}$. Photocatalytic activity of TiO₂ depends on many factors such as phase composition, crystal structure, crystallinity, crystallite size, and surface area [38]. TiO₂-300 and TiO₂-400 composed of anatase and brookite phases and there was an increase of anatase phase from 29%wt. (TiO₂-300) to 33%wt. (TiO₂-400). Commercial P25 showed higher photocatalytic activity than synthesized TiO₂ because P25 presented a higher ratio of anatase to rutile (89:11) than that of TiO₂-600 (42:30). While the particle sizes of P25 and TiO₂-600 were quite similar as $19.9 \pm 1.2 \text{ nm}$ and $18.7 \pm 3.7 \text{ nm}$, respectively. Our photocatalytic oxidation result is agreed well with the study of Ozawa et al. [39] who reported that photocatalytic activity of TiO₂ was enhanced with an increasing of percentage weight of anatase whereas the brookite phase was decreased. The anatase phase provides the highest photocatalytic activity compared to the rutile and brookite phases because anatase phase is an indirect band gap structure while the rutile and brookite phases appear to be the direct band gap one. Indirect band gap structure shows longer lifetime of electron and hole (e^- - h^+) pairs separation than direct band gap. Moreover, the anatase phase shows the highest photocatalytic activity because of the smallest particle size and the lightest effective mass of e^- - h^+ pairs which provides the fastest charge transfer to surface of TiO₂ leading to the lowest e^- - h^+ recombination [40]. Charge transfer in the different band alignments at the interfaces of TiO₂ shows high efficiency of charge separation for high photocatalytic activity under UV light conditions. The charge transfer mechanism of different phase combinations is proposed in Figure 6b–d. The mechanism of charge transfer of the mixture of anatase and brookite phases of TiO₂-300 and TiO₂-400 is shown in Figure 6b. Conduction band (CB) level can be determined from the vacuum level by using electron affinity (EA). Electron affinity of the anatase phase ($EA_A = 4.94 \text{ eV}$) is higher than that of the brookite phase ($EA_B = 4.15 \text{ eV}$). Valence band (VB) can be determined by considering energy band gap (E_g) (E_g of anatase = 3.51 eV and E_g of brookite = 3.36 eV) [41]. CB of brookite is higher than that of anatase where electrons can transfer from brookite to anatase whereas the hole conversely transfers from anatase to brookite. With increasing calcination temperature from 400 °C to 600 °C, the kinetic constant was increased from 3.87×10^{-2} to $9.46 \times 10^{-2} \text{ h}^{-1}$. The proposed charge transfer pathway in three phases of TiO₂-500 and TiO₂-600 is illustrated in Figure 6c. Electron affinity of brookite, rutile, and anatase (EA_B , EA_R , and EA_A) are 4.15, 4.73, and 4.94 eV, respectively [39]. Due to the lowest energy of EA_B , the CB of brookite is the highest level compared to those of rutile and anatase phases. Electrons can transfer from brookite to rutile and anatase between interfaces while holes transfer in the opposite direction. The mixture of three phases consists of higher interfaces than two phases leading to a longer lifetime of charge transfer and a reduction of charge recombination. Therefore, the mixture of three phases including anatase, rutile, and brookite showed higher photocatalytic activity than two phases of anatase and brookite [16,17,42]. TiO₂-600 showed higher photocatalytic activity than TiO₂-500 because TiO₂-600 consisted of higher weight percentage of anatase phase (42%wt.) than TiO₂-500 (33%wt.). With increasing calcination temperature from 600 °C to 700 °C, the kinetic constant was decreased from 9.46×10^{-2} to $6.67 \times 10^{-2} \text{ h}^{-1}$. It is interesting to note that even though the anatase phase was increased from 42%wt. (TiO₂-600) to 53%wt. (TiO₂-650),

the kinetic constant was decreased from 9.46×10^{-2} to $7.73 \times 10^{-2} \text{ h}^{-1}$. It was noticed that the crystallite size of anatase and rutile was increased from 600 °C to 650 °C as shown in Table 1. This can lead to the lower surface area of TiO₂-650 compared to that of TiO₂-600. Therefore, it is the dominance of crystallite size for the decrease of photocatalytic activity between TiO₂-600 and TiO₂-700 over the phase. The charge transfer mechanism of the mixture of anatase and rutile phases is shown in Figure 6d. Electrons in CB transfer from rutile to anatase because EA_A was higher than EA_R while holes transfer from anatase to rutile [41,43,44]. Considering the kinetic constant of TiO₂-300 ($2.54 \times 10^{-2} \text{ h}^{-1}$) and TiO₂-700 ($6.67 \times 10^{-2} \text{ h}^{-1}$), the mixture of anatase and rutile (TiO₂-700) provided higher photocatalytic activity than that of anatase and brookite (TiO₂-300). It was observed that the weight percentage of anatase phase of TiO₂-700 (38%wt.) was higher than that of TiO₂-300 (29%wt.) while the crystallite size of TiO₂-300 was smaller than that of TiO₂-700. High crystallinity of the mixture of anatase and rutile phases provided higher photocatalytic activity than that of the mixture of anatase and brookite phases because it has been reported that TiO₂ comprising the brookite phase of more than 25% could inhibit photocatalytic activity of TiO₂ [45]. At calcination temperature of 800 °C, it shows the lowest kinetic constant of $2.19 \times 10^{-2} \text{ h}^{-1}$ because TiO₂-800 consisted of only rutile phase and had the largest crystallite size of 52 nm. Due to the direct band gap structure of the rutile phase, there is the fast recombination of e^-h^+ pairs as shown in Figure 6e leading to the lowest photocatalytic activity of TiO₂-800. These results correlated well with the study of Zhang et al. [46] who found that photocatalytic activity of H₂ evolution of the pure rutile phase was lower than that of the mixture of anatase and rutile phases.

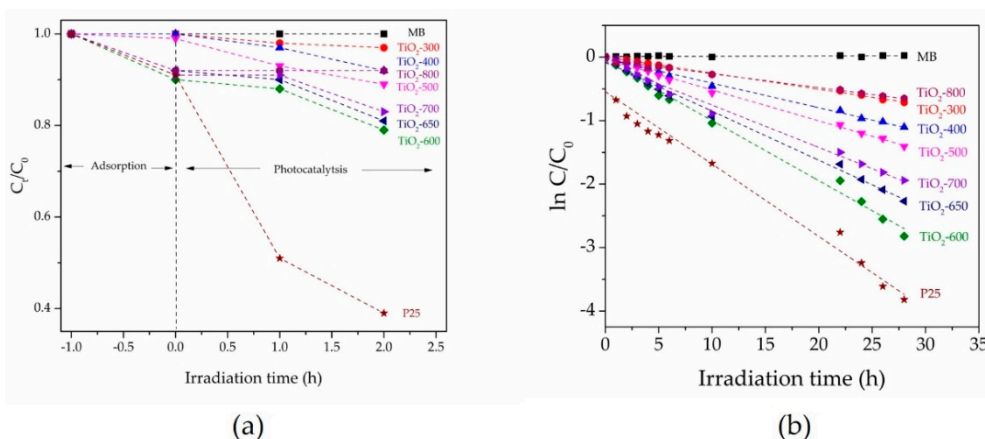
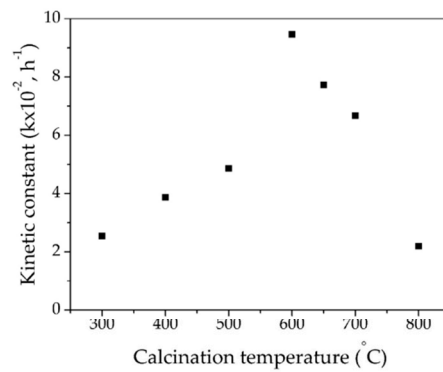


Figure 5. (a) The adsorption change of methylene blue (MB) in the dark and photocatalytic degradation of MB under UV light for 2 h with the synthesized TiO₂ and P25. (b) Photocatalytic degradation of MB under UV light obtained when using synthesized TiO₂ with different calcination temperatures.

Table 3. Kinetic constant (k) of MB degradation obtained when using synthesized TiO₂ powder with different calcination temperatures.

Calcination Temperature (°C)	300	400	500	600	650	700	800	P25
Kinetic constant ($k \times 10^{-2}$) (h^{-1})	2.54	3.87	4.86	9.46	7.73	6.67	2.19	11.41



(a)

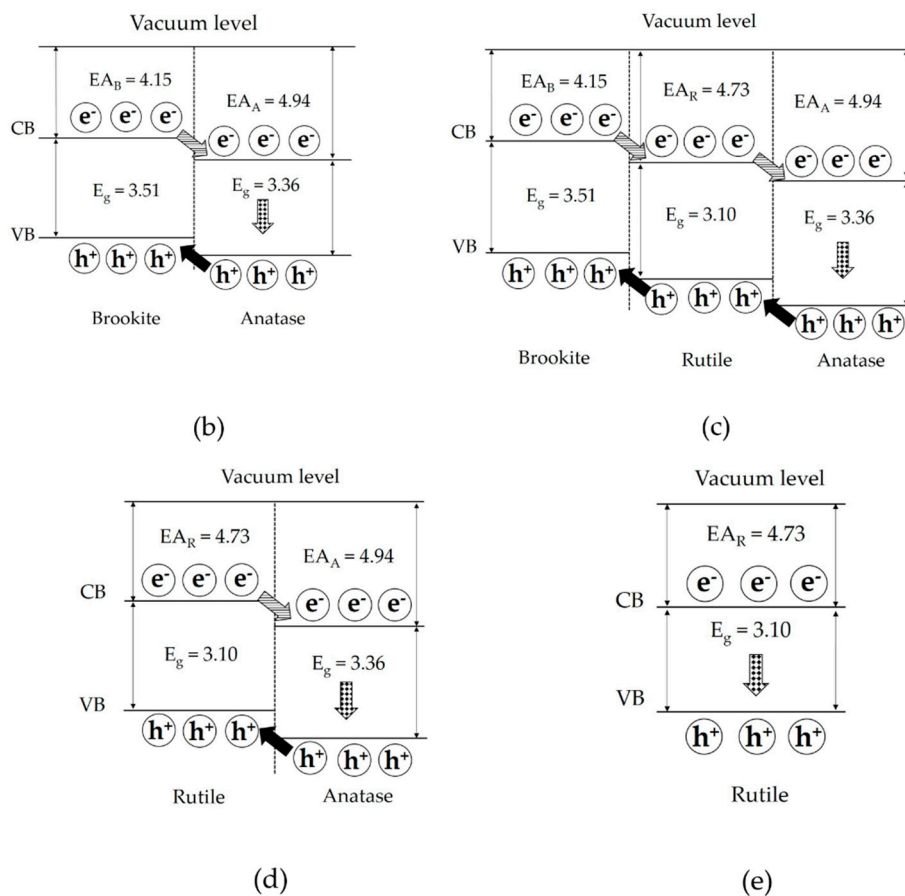


Figure 6. (a) Photocatalytic activity of TiO₂ presenting the kinetic constant at of TiO₂ as a function of calcination temperatures from 300 °C to 800 °C. Proposed mechanisms of different conduction and valence band alignments of (b) anatase–brookite, (c) anatase–rutile–brookite, (d) anatase–rutile, and (e) rutile phase. Striped and black arrows show electron transfer in conduction band and hole transfer in valence band, respectively. Checkerboard arrow represents a recombination of electrons and holes.

4. Conclusions

The effect of calcination temperature plays an essential role on particle size, phase transition, crystallinity, and crystallite size of synthesized TiO₂ via the WBMS method. Narrow size distribution of TiO₂ nanoparticles could be obtained. A mixture of brookite and anatase phases was found at calcination temperature less than 400 °C. The rutile phase was found above 500 °C. The mixture of anatase, rutile, and brookite phases was obtained at calcination temperature between 500 °C

and 600 °C. Anatase and brookite phases were completely transferred to the rutile phase at 800 °C. Phase composition and crystallite size are important factors for high photocatalytic activity. The high percentage weight of the anatase phase had a strong effect on the photocatalytic activity between 300 °C and 600 °C while the crystallite and particle size of TiO₂ had a dominant influence on the photocatalytic activity from 600 °C to 700 °C. The highest photocatalytic activity with three phases of TiO₂-600 was achieved with kinetic constant of $9.46 \times 10^{-2} \text{ h}^{-1}$. The highest photocatalytic activity in this study can be applied for environmental application such as water decontamination or pollutants removal from water.

Author Contributions: Conceptualization, T.E. and C.S.; methodology, T.E. and C.S.; validation, S.P., T.W. and P.K.; investigation, S.P., T.W. and P.K.; formal analysis, S.P., C.S. and T.E.; resources, P.K.; writing—original draft preparation, S.P.; writing—review and editing, T.E. and C.S.; supervision, T.E. and C.S.; funding acquisition, T.E. and C.S. All authors have read and agreed to the published version of the manuscript.

Funding: This work was financially supported by the National Nanotechnology Center (NANOTEC), National Science and Technology Development Agency (NSTDA) (grant number P1850142). This study was also funded by Thailand Graduate Institute of Science and Technology (TGIST) (grant number SCA-CO-2560-4582-TH).

Conflicts of Interest: The authors declare no conflict of interest.

References

1. Park, H.K.; Kim, D.K.; Kim, C.H. Effect of solvent on titania particle formation and morphology in thermal hydrolysis of TiCl₄. *J. Am. Ceram. Soc.* **1997**, *80*, 743–749. [[CrossRef](#)]
2. Boisvert, J.-P.; Persello, J.; Foissy, A.; Castaing, J.-C.; Cabane, B. Effect of surface charge on the adsorption mode of sodium poly (acrylate) on alumina-coated TiO₂ used as coating pigment. *Colloids Surf. A* **2000**, *168*, 287–296. [[CrossRef](#)]
3. Meléndez-Ceballos, A.; Fernández-Valverde, S.M.; Barrera-Díaz, C.; Albin, V.; Lair, V.; Ringuedé, A.; Cassir, M. TiO₂ protective coating processed by atomic layer deposition for the improvement of MCFC cathode. *Int. J. Hydrog. Energy* **2013**, *38*, 13443–13452. [[CrossRef](#)]
4. Jacobs, J.F.; van de Poel, I.; Osseweijer, P. Sunscreens with titanium dioxide (TiO₂) nano-particles: A societal experiment. *Nanoethics* **2010**, *4*, 103–113. [[CrossRef](#)] [[PubMed](#)]
5. Verdier, T.; Coutand, M.; Bertron, A.; Roques, C. Antibacterial activity of TiO₂ photocatalyst alone or in coatings on *E. coli*: The influence of methodological aspects. *Coatings* **2014**, *4*, 670–686. [[CrossRef](#)]
6. Siah, W.R.; Lintang, H.O.; Shamsuddin, M.; Yuliati, L. In High photocatalytic activity of mixed anatase-rutile phases on commercial TiO₂ nanoparticles. *IOP Conf. Ser. Mater. Sci. Eng. IOP Publ.* **2016**, 012005. [[CrossRef](#)]
7. Li, L.; Yan, J.; Wang, T.; Zhao, Z.-J.; Zhang, J.; Gong, J.; Guan, N. Sub-10 nm rutile titanium dioxide nanoparticles for efficient visible-light-driven photocatalytic hydrogen production. *Nat. Commun.* **2015**, *6*, 5881. [[CrossRef](#)]
8. Ohno, T.; Tokieda, K.; Higashida, S.; Matsumura, M. Synergism between rutile and anatase TiO₂ particles in photocatalytic oxidation of naphthalene. *Appl. Catal. A* **2003**, *244*, 383–391. [[CrossRef](#)]
9. El Gaidoumi, A.; Doña Rodríguez, J.M.; Pulido Melián, E.; González-Díaz, O.M.; Navío Santos, J.A.; El Bali, B.; Kherbeche, A. Synthesis of sol-gel pyrophyllite/TiO₂ heterostructures: Effect of calcination temperature and methanol washing on photocatalytic activity. *Surf. Interfaces* **2019**, *14*, 19–25. [[CrossRef](#)]
10. Arbuj, S.S.; Hawaldar, R.R.; Mulik, U.P.; Wani, B.N.; Amalnerkar, D.P.; Waghmode, S.B. Preparation, characterization and photocatalytic activity of TiO₂ towards methylene blue degradation. *Mater. Sci. Eng. B* **2010**, *168*, 90–94. [[CrossRef](#)]
11. Lv, K.; Yu, J.; Deng, K.; Li, X.; Li, M. Effect of phase structures on the formation rate of hydroxyl radicals on the surface of TiO₂. *J. Phys. Chem. Solids* **2010**, *71*, 519–522. [[CrossRef](#)]
12. Kandiel, T.A.; Robben, L.; Alkaim, A.; Bahnemann, D. Brookite versus anatase TiO₂ photocatalysts: Phase transformations and photocatalytic activities. *Photochem. Photobiol. Sci.* **2013**, *12*, 602–609. [[CrossRef](#)] [[PubMed](#)]
13. Tay, Q.; Liu, X.; Tang, Y.; Jiang, Z.; Sum, T.C.; Chen, Z. Enhanced photocatalytic hydrogen production with synergistic two-phase anatase/brookite TiO₂ nanostructures. *J. Phys. Chem. C* **2013**, *117*, 14973–14982. [[CrossRef](#)]

14. Cao, Y.; Li, X.; Bian, Z.; Fuhr, A.; Zhang, D.; Zhu, J. Highly photocatalytic activity of brookite/rutile TiO₂ nanocrystals with semi-embedded structure. *Appl. Catal. B Environ.* **2016**, *180*, 551–558. [[CrossRef](#)]
15. Štengl, V.; Králová, D. Photoactivity of brookite–rutile TiO₂ nanocrystalline mixtures obtained by heat treatment of hydrothermally prepared brookite. *Mater. Chem. Phys.* **2011**, *129*, 794–801. [[CrossRef](#)]
16. Di Paola, A.; Bellardita, M.; Ceccato, R.; Palmisano, L.; Parrino, F. Highly active photocatalytic TiO₂ powders obtained by thermohydrolysis of TiCl₄ in water. *J. Phys. Chem. C* **2009**, *113*, 15166–15174. [[CrossRef](#)]
17. Liao, Y.; Que, W.; Jia, Q.; He, Y.; Zhang, J.; Zhong, P. Controllable synthesis of brookite/anatase/rutile TiO₂ nanocomposites and single-crystalline rutile nanorods array. *J. Mater. Chem.* **2012**, *22*, 7937–7944. [[CrossRef](#)]
18. Gomathi Thanga Keerthana, B.; Solaiyammal, T.; Muniyappan, S.; Murugakoothan, P. Hydrothermal synthesis and characterization of TiO₂ nanostructures prepared using different solvents. *Mater. Lett.* **2018**, *220*, 20–23. [[CrossRef](#)]
19. Falk, G.S.; Borlaf, M.; López-Muñoz, M.J.; Fariñas, J.C.; Rodrigues Neto, J.B.; Moreno, R. Microwave-assisted synthesis of TiO₂ nanoparticles: Photocatalytic activity of powders and thin films. *J. Nanopart. Res.* **2018**, *20*, 23. [[CrossRef](#)]
20. Da Silva, E.P.; Winkler, M.E.G.; Giufrida, W.M.; Cardozo-Filho, L.; Alonso, C.G.; Lopes, J.B.O.; Rubira, A.F.; Silva, R. Effect of phase composition on the photocatalytic activity of titanium dioxide obtained from supercritical antisolvent. *J. Colloid Interface Sci.* **2019**, *535*, 245–254. [[CrossRef](#)]
21. Behnajady, M.A.; Eskandarloo, H. Preparation of TiO₂ nanoparticles by the sol–gel method under different pH conditions and modeling of photocatalytic activity by artificial neural network. *Res. Chem. Intermed.* **2015**, *41*, 2001–2017. [[CrossRef](#)]
22. Lopez, L.; Daoud, W.A.; Dutta, D. Preparation of large scale photocatalytic TiO₂ films by the sol–gel process. *Surf. Coat. Technol.* **2010**, *205*, 251–257. [[CrossRef](#)]
23. Jung, H.J.; Sohn, Y.; Sung, H.G.; Hyun, H.S.; Shin, W.G. Physicochemical properties of ball milled boron particles: Dry vs. wet ball milling process. *Powder Technol.* **2015**, *269*, 548–553. [[CrossRef](#)]
24. Jung, H.J.; Nam, K.; Sung, H.-G.; Hyun, H.S.; Sohn, Y.; Shin, W.G. Preparation of TiO₂-decorated boron particles by wet ball milling and their photoelectrochemical hydrogen and oxygen evolution reactions. *Materials* **2016**, *9*, 1012. [[CrossRef](#)] [[PubMed](#)]
25. Behnajady, M.A.; Eskandarloo, H.; Modirshahla, N.; Shokri, M. Investigation of the effect of sol–gel synthesis variables on structural and photocatalytic properties of TiO₂ nanoparticles. *Desalination* **2011**, *278*, 10–17. [[CrossRef](#)]
26. Mutuma, B.K.; Shao, G.N.; Kim, W.D.; Kim, H.T. Sol–gel synthesis of mesoporous anatase–brookite and anatase–brookite–rutile TiO₂ nanoparticles and their photocatalytic properties. *J. Colloid Interface Sci.* **2015**, *442*, 1–7. [[CrossRef](#)]
27. Yu, J.-G.; Yu, H.-G.; Cheng, B.; Zhao, X.-J.; Yu, J.C.; Ho, W.-K. The effect of calcination temperature on the surface microstructure and photocatalytic activity of TiO₂ thin films prepared by liquid phase deposition. *J. Phys. Chem. B* **2003**, *107*, 13871–13879. [[CrossRef](#)]
28. Choi, H.; Kim, Y.J.; Varma, R.S.; Dionysiou, D.D. Thermally stable nanocrystalline TiO₂ photocatalysts synthesized via sol–gel methods modified with ionic liquid and surfactant molecules. *Chem. Mater.* **2006**, *18*, 5377–5384. [[CrossRef](#)]
29. Phromma, S.; Sapcharoenkun, C.; Wutikhun, T.; Kasamechonchung, P.; Eksangsri, T. Synthesis of TiO₂ nanoparticles with high photocatalytic activity by wet ball milling sol-gel method. In Proceedings of the Innovative Chemical Engineering and Technology toward a Sustainable Future, Bangkok, Thailand, 18–20 October 2017; Volume 7, pp. 211–214.
30. Bahadur, J.; Agrawal, S.; Panwar, V.; Parveen, A.; Pal, K. Antibacterial properties of silver doped TiO₂ nanoparticles synthesized via sol-gel technique. *Macromol. Res.* **2016**, *24*, 488–493. [[CrossRef](#)]
31. Rauf, A.; Shah, M.S.A.S.; Lee, J.Y.; Chung, C.-H.; Bae, J.W.; Yoo, P.J. Non-stoichiometric SnS microspheres with highly enhanced photoreduction efficiency for Cr (VI) ions. *RSC Adv.* **2017**, *7*, 30533–30541. [[CrossRef](#)]
32. Hu, Y.; Tsai, H.L.; Huang, C.L. Effect of brookite phase on the anatase–rutile transition in titania nanoparticles. *J. Eur. Ceram. Soc.* **2003**, *23*, 691–696. [[CrossRef](#)]
33. Bamne, J.; Taiwade, K.; Sharma, P.K.; Haque, F. Effect of calcination temperature on the growth of TiO₂ nanoparticle prepared via sol-gel method using triton X-100 as surfactant. *AIP Conf Proc.* **2018**, *2039*, 0200761–0200765. [[CrossRef](#)]

34. Saalinraj, S.; Ajithprasad, K.C. Effect of Calcination Temperature on Non-linear Absorption Co-efficient of Nano Sized Titanium Dioxide (TiO₂) Synthesised by Sol-Gel Method. *Mater. Today Proc.* **2017**, *4*, 4372–4379. [[CrossRef](#)]
35. Banjuraizah, J.; Ong, Y.; Ahmad, Z. Effect of Calcination Temperature on Titanium Dioxide Synthesized by Sol-Gel Method. *Int. J. Cur. Res. Eng. Sci. Tech.* **2018**, *1*, 68–74. [[CrossRef](#)]
36. Calandra, P.; Lombardo, D.; Pistone, A.; Liveri, V.; Trusso, S. Structural and optical properties of novel surfactant-coated Yb@TiO₂ nanoparticles. *J. Nanopart. Res.* **2011**, *13*, 5833–5839. [[CrossRef](#)]
37. Calandra, P.; Ruggirello, A.; Pistone, A.; Liveri, V. Structural and Optical Properties of Novel Surfactant Coated TiO₂–Ag Based Nanoparticles. *J. Cluster Sci.* **2010**, *21*, 767–778. [[CrossRef](#)]
38. Baiju, K.V.; Shukla, S.; Sandhya, K.S.; James, J.; Warriar, K.G.K. Photocatalytic Activity of Sol–Gel-Derived Nanocrystalline Titania. *J. Phys. Chem. C* **2007**, *111*, 7612–7622. [[CrossRef](#)]
39. Ozawa, T.; Iwasaki, M.; Tada, H.; Akita, T.; Tanaka, K.; Ito, S. Low-temperature synthesis of anatase–brookite composite nanocrystals: The junction effect on photocatalytic activity. *J. Colloid Interface Sci.* **2005**, *281*, 510–513. [[CrossRef](#)]
40. Zhang, J.; Zhou, P.; Liu, J.; Yu, J. New understanding of the difference of photocatalytic activity among anatase, rutile and brookite TiO₂. *Phys. Chem. Chem. Phys.* **2014**, *16*, 20382–20386. [[CrossRef](#)]
41. Buckeridge, J.; Butler, K.T.; Catlow, C.R.A.; Logsdail, A.J.; Scanlon, D.O.; Shevlin, S.A.; Woodley, S.M.; Sokol, A.A.; Walsh, A. Polymorph Engineering of TiO₂: Demonstrating How Absolute Reference Potentials Are Determined by Local Coordination. *Chem. Mater.* **2015**, *27*, 3844–3851. [[CrossRef](#)]
42. Preethi, L.; Mathews, T.; Nand, M.; Jha, S.; Gopinath, C.S.; Dash, S. Band alignment and charge transfer pathway in three phase anatase-rutile-brookite TiO₂ nanotubes: An efficient photocatalyst for water splitting. *Appl. Catal. B* **2017**, *218*, 9–19. [[CrossRef](#)]
43. Hurum, D.C.; Agrios, A.G.; Gray, K.A.; Rajh, T.; Thurnauer, M.C. Explaining the enhanced photocatalytic activity of degussa P25 Mixed-phase TiO₂ using EPR. *J. Phys. Chem. B* **2003**, *107*, 4545–4549. [[CrossRef](#)]
44. Mi, Y.; Weng, Y. Band alignment and controllable electron migration between rutile and anatase TiO₂. *Sci. Rep.* **2015**, *5*, 11482. [[CrossRef](#)]
45. Zhao, H.; Liu, L.; Andino, J.M.; Li, Y. Bicrystalline TiO₂ with controllable anatase–brookite phase content for enhanced CO₂ photoreduction to fuels. *J. Mater. Chem. A* **2013**, *1*, 8209–8216. [[CrossRef](#)]
46. Zhang, J.; Xu, Q.; Feng, Z.; Li, M.; Li, C. Importance of the relationship between surface phases and photocatalytic activity of TiO₂. *Angew. Chem. Int. Ed.* **2008**, *47*, 1766–1769. [[CrossRef](#)]



© 2020 by the authors. Licensee MDPI, Basel, Switzerland. This article is an open access article distributed under the terms and conditions of the Creative Commons Attribution (CC BY) license (<http://creativecommons.org/licenses/by/4.0/>).